Received 10 March 2022; revised 22 March 2022; accepted 27 March 2022. Date of publication 11 April 2022; date of current version 27 April 2022.

Digital Object Identifier 10.1109/OJAP.2022.3166232

Design of Microfluidic Reflectarray Elements for Multi-Reconfiguration Using Liquid Metal

EDUARDO CARRASCO[1] (Senior Member, IEEE), JUAN GOMEZ-CRUZ[2] (Member, IEEE), MARIO SERRANO-BERRUECO[1], CARLOS E. SAAVEDRA[3], AND CARLOS ESCOBEDO[2] (Member, IEEE)

[1]Information Processing and Telecommunications Center, Universidad Politécnica de Madrid, 28040 Madrid, Spain

[2]Department of Chemical Engineering, Queen's University, Kingston, ON K7L 3N6, Canada

[3]Department of Electrical Engineering, Queen's University, Kingston, ON K7L 3N6, Canada

CORRESPONDING AUTHORS: E. CARRASCO AND C. ESCOBEDO (e-mail: eduardo.carrasco@upm.es; ce32@queensu.ca)

This work was supported in part by the Spanish Ministry of Science and Innovation and the Spanish Agency for Research within Project ENHANCE-5G under Grant PID2020-114172RB-C22/AEI/10.13039/501100011033, and in part by the Spanish Ministry of Economic Affairs and Digital Transformation by the Next Generation EU under the Recovery plan for Europe and the Recovery and Resilience Facility, within the Project DISRADIO TSI-063000-2021-82. The work of Carlos Escobedo was supported in part by the Natural Sciences and Engineering Research Council of Canada under Grant RGPIN-2019-04292, and in part by the Canada Foundation for Innovation John R. Evans Leaders' Fund Program under Grant 319670.

ABSTRACT Using an alloy of non-toxic liquid metal (Galinstan) is proposed to implement multi-reconfiguration in reflectarray elements. Reflectarray antennas are an interesting technology for dynamically controlling, simultaneously or individually, different properties of the antenna (beam shape and pointing direction, field polarization, and frequency of operation) according to the system's demand. The use of liquid metal, which can potentially be used to re-shape the topology of the unit cell, along with advances in the micro-and nanofluidics field, provides more flexibility for efficiently implementing such multi-reconfiguration. A frequency-reconfigurable reflectarray element is based on the well-known aperture-coupled cell, and a phase-reconfigurable cell based on single-and multi-resonance dipoles is proposed at 28 GHz. One advantage of microfluidics is that the concept can easily be extended to much higher frequencies, where other devices start to be expensive, inefficient, or limited in terms of multi-reconfiguration. The microfluidic technology required to implement the dipole-based element is demonstrated using a microfluidic burst-valve chip. Additionally, a simplified RF proof-of-concept is presented using the well-known waveguide simulator technique from 15 GHz to 22 GHz (WR51). The results obtained constitute an important first step toward the implementation of multi-reconfigurable reflectarray antennas.

INDEX TERMS Antennas, reflectarray, reconfiguration, microfluidics, liquid metal, PDMS.

I. INTRODUCTION

REFLECTARRAY antennas combine the main features of parabolic reflectors and planar arrays [1], highlighting the low losses, low cross-polarization, moderate profile, and the possibility of implementing dynamic reconfiguration [2]. This reconfiguration has traditionally focused on steering or changing the beam shape. In recent years, there has been a considerable need for antenna systems with total flexibility not only in terms of spatial reconfiguration, but also in terms of polarization and frequency reconfiguration [3]–[4].

Derived from their application over almost two decades in chemistry, biology, and medicine, microfluidics-based technology offers a wide range of micro-devices such as valves, mixers, pumps, and even lab-on-chip systems [5]–[6]. These devices and their associated fluid materials can be exploited to manipulate the electrical properties of antennas.

Microfluidics, the field dedicated to studying the behavior of fluids in microstructures, has found a broad range of applications over the past two decades. In addition to the inherent benefits of microfluidics, they include the precise control of microenvironments, use of minimal amounts of reagents to replicate macroscopic experimental conditions, high-throughput analysis, and the use of non-inertial forces to actuating fluids at a small scale [7]. Microfluidics has recently permeated the telecommunications field, enabling the development of reconfigurable elements, including liquid-reconfigurable patch antennas [8], reconfigurable microstrip antennas for switchable multiband systems [9], and wideband slotted bow-tie antennas [10].

The use of a fluidic-based approach to reconfigure only the phase of a reflectarray cell was proposed in [11]. The element was based on a coaxial stub microfluidic impedance transformer operating at 3 GHz. Reactive loading of the microstrip reflectarray element was used to achieve low-loss and continuous phase control over the radiated signal. The cell acted with the remotely manipulated flow of colloidal dispersions beneath the antenna's ground plane. Adjustments of the nanoparticle concentration in the dielectric fluid alter the permittivity, allowing the phase to be controlled by reflection.

One alternative to dielectric fluids is the use of liquid metal, which has been identified as a very interesting solution for radiating elements in reflectarrays because they have both the conductivity of metal and the fluidic properties of a liquid, allowing the re-shaping of the element, thereby introducing the possibility of dynamic reconfiguration. This reconfiguration can be implemented in terms of frequency, polarization, phase, or even a combination of these.

Owing to the toxicity of other liquid metals, in this work, the use of a non-toxic metal alloy made of 68.5% gallium (Ga), 21.5% indium (In), and 10% tin (Sn) [12], known as Galinstan, with electrical conductivity of $2.3{\cdot}10^6$ S/m and melting point around $-19°$C, is proposed. To the best of our knowledge, this is the first time Galinstan has been proposed to implement reconfiguration in reflectarray elements.

This material has been successfully used in single-patch antennas at 2.4 GHz [13]. In [14], a broadband monopole antenna was designed for stretchable electronics. The antenna consists of a liquid conductor for the radiating element and SEBS (Styrene-Ethylene-Butylene-Styrene) for the antenna substrate, showing a maximum gain of 4.63 dBi at 5.8 GHz. A polarization-reconfigurable liquid dielectric resonator antenna (DRA) incorporating liquid metal was designed in [15]. The container comprises two zones: one is the liquid dielectric zone for ethyl acetate and the second zone is filled with Galinstan. A reconfigurable liquid-metal dipole antenna was presented in [16]. By changing the position of Galinstan, five discrete states with varying polarization states and null directions were obtained.

The incursion of microfluidics to the applied electromagnetic field is still emerging. The development of new technology based on the amalgamation of fields will most likely grow significantly in the next few years. In this study, we introduce microfluidic-based reflectarray elements that can be reconfigured upon the actuation of liquid metals, including a proof-of-concept of the microfluidic burst valve, which is the first in the reflectarray antenna field.

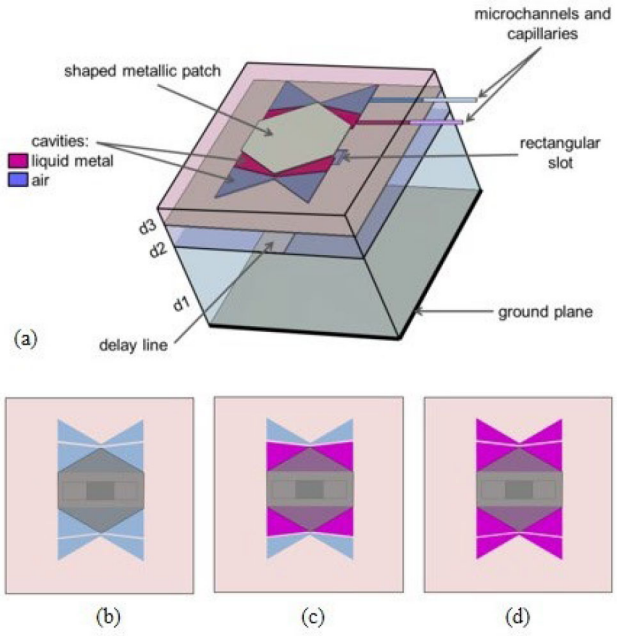

FIGURE 1. Proposed element for frequency reconfiguration (a) Expanded view and four-cavity configurations for upper, central and lower frequencies from (b) All empty. (c) Two filled. (d) Four filled.

II. LIQUID METAL AS RECONFIGURATION MATERIAL IN REFLECTARRAY ANTENNAS

Two different elements are analyzed in the following sections to determine the feasibility of using Galinstan in reflectarray antennas. The first topology is based on the well-known aperture-coupled configuration, in which the usual square patch is replaced by an optimized patch whose shape can be varied by injecting Galinstan into a discrete number of cavities. The shaping of the patch allows for dynamic frequency tuning. The second topology is based on a resonant dipole whose length can be adjusted to control the phase of the reflected field at the element level. The introduction of more dipoles improves the bandwidth of the cell.

A. FREQUENCY RECONFIGURATION IN APERTURE-COUPLED ELEMENTS

Owing to its fluidic behavior, Galinstan can be easily displaced into microchannels, modifying the shape of a metallic layer into a reflectarray cell. In this subsection, a frequency reconfigurable element is proposed in the frequency band from 25.75 GHz to 34.50 GHz.

The proposed topology is shown in Fig. 1, and the dimensions are listed in Table 1. It consists of a delay line coupled through a rectangular slot to a metallic patch with an optimized hexahedron shape. While the dynamic

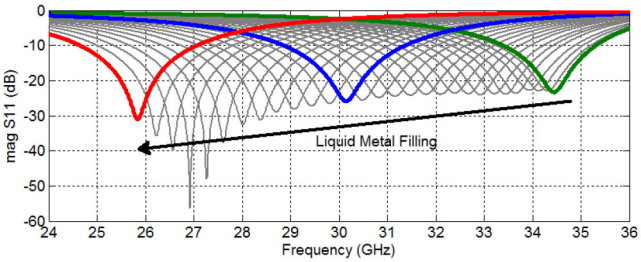

FIGURE 2. Matching of the proposed reflective cell for different volumes of the liquid metal (25.85 GHz, 30.15 GHz, 34.45 GHz, intermediate frequencies).

TABLE 1. Dimensions for the element with frequency reconfiguration.

	Dimensions [mm]
Cell size	5.00
D1 thickness	2.5
D2 thickness	0.635
D3 thickness	0.508
Microfluidic thickness	0.034
Hexagonal patch side (vertical side)	1.0
Hexagonal patch side (oblique sides)	1.3
Slot length/width	2.1/0.5
Microstrip line length/width	0.9
Microstrip offset respect to center	0.78

phase control produced by this topology has been widely demonstrated [17]–[19], here, the effort is focused on dynamically controlling the operation frequency, as this control can be implemented independently. Notably, this element can be simultaneously reconfigured in phase if a second control mechanism is implemented in the delay line (using lumped elements or Galinstan again). For the frequency-reconfigurable element, the patch consisted of a copper section printed on the upper substrate (d3, $\varepsilon_r = 2.33$, $\tan\delta = 0.0012$) and a discrete number of 34-μm-thick cavities, situated 50μm inside the substrate. The cavities and their associated microchannels can be fabricated using a combined process of laser ablation and lamination, which is a common process in microfluidics, or using a high-resolution additive manufacturing technique. These cavities can be dynamically filled or emptied to Galinstan. The slot and microstrip line in the proposed topology share a common dielectric (D2, $\varepsilon_r = 6$, $\tan\delta = 0.0023$), whereas the spacer for placing the ground plane is a foam ($\varepsilon_r = 1.05$, $\tan\delta = 0.0017$). In the proposed reflectarray element, the operating frequency can be adjusted according to the shape and number of pairs of cavities and their states (filled or empty). Fig. 2 shows the simulated matching at the input of the microstrip line for different volumes of liquid metal obtained with CST Studio Suite and infinite array boundaries. Designing an element assuming a well-matched delay line is a common strategy for obtaining broadband aperture-coupled elements [20]. An open microstrip line replaced the matched line in a further step. In Fig. 2, the green, blue, and red curves correspond to the cases illustrated in Fig. 1 using four cavities: (b) empty cavities, (c) filled cavities, and (d) filled cavities.

TABLE 2. Dimensions for basic element with single dipole.

	Dimensions [mm]
Cell size	5.35
PDMS bottom layer thickness	1.2
PDMS top layer thickness	0.2
Microfluidic channel thickness	0.03
Microfluidic channel length	0.1
Microfluidic channel width	0.07
Dipole width	0.6
Segment 1 length	2
Segments 2-7 length	0.15
Segments 8-9 length	0.78

In practice, the operating frequencies of all the cells in the reflectarray are the same. This feature simplifies the frequency control. All the elements must be filled with the same quantity of liquid metal; therefore, a simple filling mechanism is required to tune the operation frequency. It is worth mentioning that the number of available frequencies can be increased by having more cavities that produce intermediate states (grey curves).

As mentioned, the previous element can also be used for implementing phase reconfiguration simultaneously with frequency reconfiguration if Galinstan is also used to change the electrical length of the delay line, in a manner similar to that described in the following dipole-based elements.

For the scope of this work, it is assumed that the frequency switching time is not a constraint in the system but is a constraint to be optimized according to the actuation system.

B. PHASE RECONFIGURATION IN DIPOLE BASED ELEMENTS

Dipole elements have been proposed as efficient elements in reflectarray antennas for fixed-[21] and reconfigurable-beam applications [22]. Using this topology but replacing the dipole metallization with a Galinstan-filled microfluidic channel allows phase reconfiguration to be obtained, and opens the door to more complex topologies that also allow reconfiguring the frequency or polarization. The general scheme of the proposed element with dynamic phase control working at a central frequency of 28 GHz is shown in Fig. 3(a). The element consisted of two layers: a dielectric substrate and a ground plane at the back face. The ground plane was modeled as a perfect electrical conductor (PEC) with zero thickness. The material used for the substrate was PDMS, whose electrical permittivity and losses are given by $\varepsilon_r = 2.77$ and $\tan\delta = 0.0127$. The microfluidic channel through which Galinstan moved was located at the top of the lower PDMS layer and had a thickness of 30 μm. An electrical conductivity of $\sigma = 2.3 \cdot 10^6\ S/m$ is considered for Galinstan.

The optimized element is shown in Fig. 3 and corresponds to the dimensions listed in Table 2. A segment is filled with Galinstan for each state, starting with the one down (red) and then filling in a sequential manner the segments (blue,

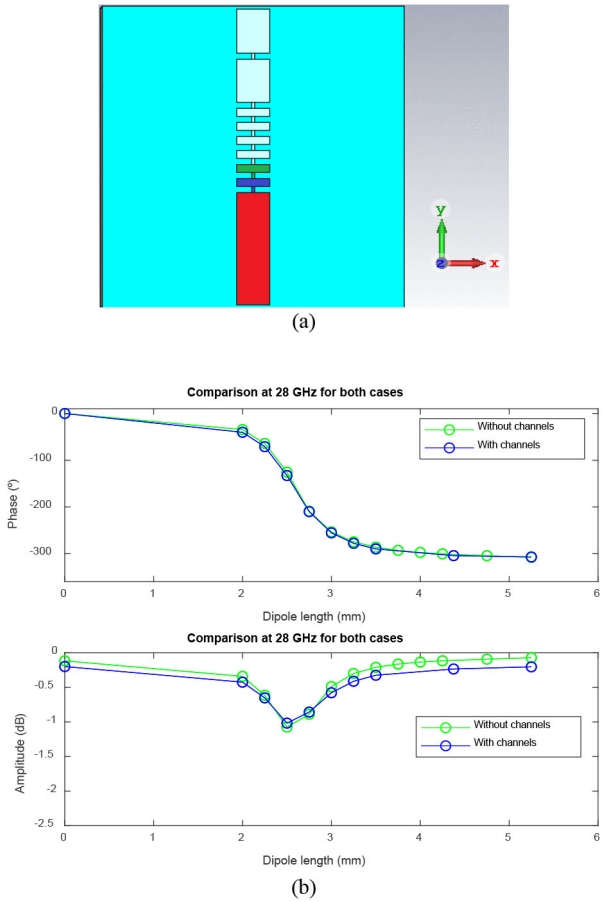

FIGURE 3. Single dipole element. (a) Front view with micro-channels. (b) Phase and amplitude of the reflection coefficient for simple model and detailed model (considering the interconnection microchannels).

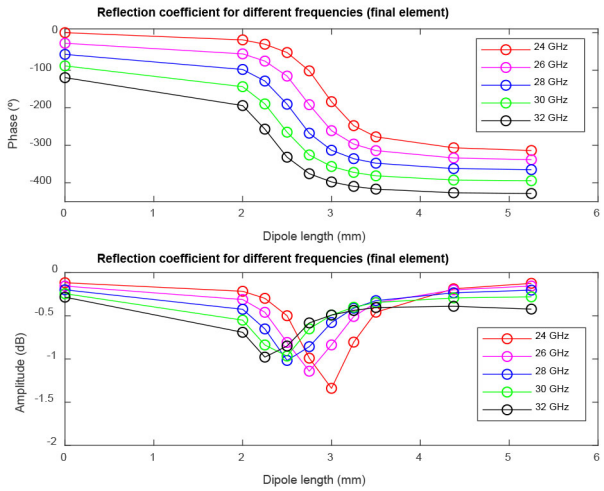

FIGURE 4. Reflection coefficient obtained with the optimized element as a function of the dipole length for different frequencies.

TABLE 3. Dimensions for optimized broadband dipole based element.

	Dimensions [mm]
Cell size	5.35
PDMS bottom layer thickness	1.2
PDMS top layer thickness	0.2
Microfluidic channel thickness	0.03
Microfluidic channel length	0.1
Microfluidic channel width	0.07
Dipole width	0.4
Central segment 1 length	2.02
Central segments 2-8 length	0.23
Central segments 9-10 length	0.35
Separation from center to center	1.64
Scale factor	0.6 (no units)
Lateral segment 1 length	1.21
Lateral segments 2-8 length	0.1
Lateral segments 9-10 length	0.17

then green, etc.). As can be seen, the dipole length is discretized with more resolution in the zones in which the change of phase is more important. Fig. 3(b) shows the phase and amplitude of the reflected wave as a function of the dipole length, comparing a simple model (continuous dipole, neglecting the interconnection channels) with a detailed model (considering the effect of the microchannels). The simulations were performed using CST Studio Suite, again considering the mutual coupling between the elements. As can be seen, the results don't change when the microchannels are introduced. However, a dependence starts to appear as the microchannels become larger; therefore, they must be considered in the design.

Fig. 4 shows the simulated results for the case that considers the microchannels in a broadband range from 24 GHz to 32 GHz. Although the 360° phase range is practically obtained in the entire band, the phase variation as a function of the dipole length has an abrupt response. This change limits the bandwidth of the element and also reduces the tolerance limit in the fabrication because a small error in the length of the dipole can produce an important change in the phase, increasing the phase errors in the design of an antenna.

A common solution for increasing the bandwidth in reflectarray antennas when resonant elements are used is to use more dipoles in the same cell but with a slightly different resonant frequency. This allowed us to obtain a linear variation of the phase as a function of the dipole length in a broadband. A reflectarray element using microfluidic technology with Galinstan as a liquid metal was optimized using three dipoles. Table 3 shows the element's dimensions, in which two identical dipoles are collocated to the sides of a central dipole. The lateral dipoles were scaled by a factor of 0.6, and all were filled with Galinstan sequentially from the first segment (red). As shown in Fig. 5(b), the phase response has a linear dependence on the central dipole length, and the phase range is increased to more than 500° in a wide band. This element demonstrates the potential use of Galinstan together with microfluidic technology to control the phase of a reflected wave in reflectarray antennas and will be used as the baseline for the micro-dynamic burst microvalves proposed and demonstrated in the following sections.

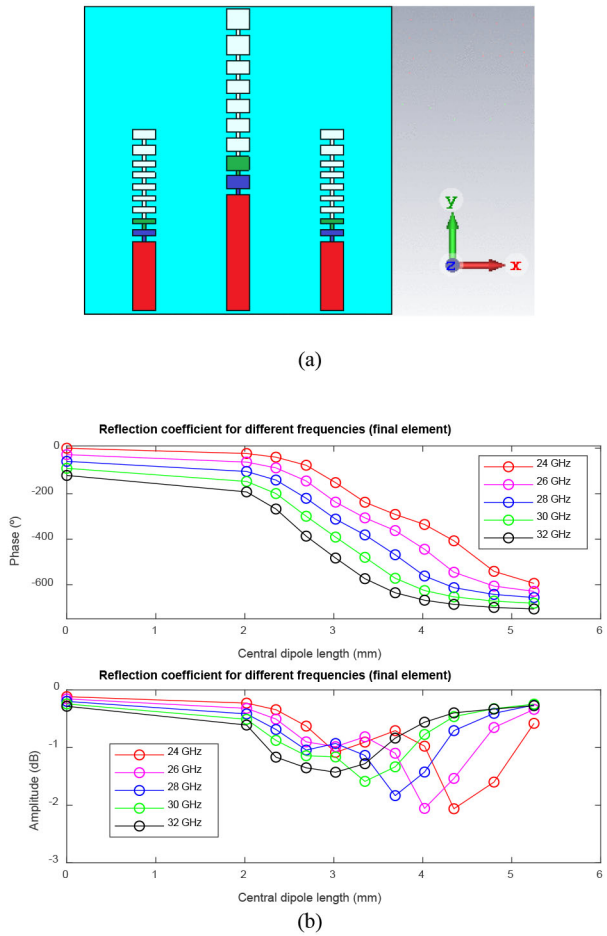

FIGURE 5. Broadband element with three dipoles. (a) Front view with micro-channels. (b) The reflection coefficient's phase and amplitude as a function of the central dipole length, from 24 GHz to 32 GHz.

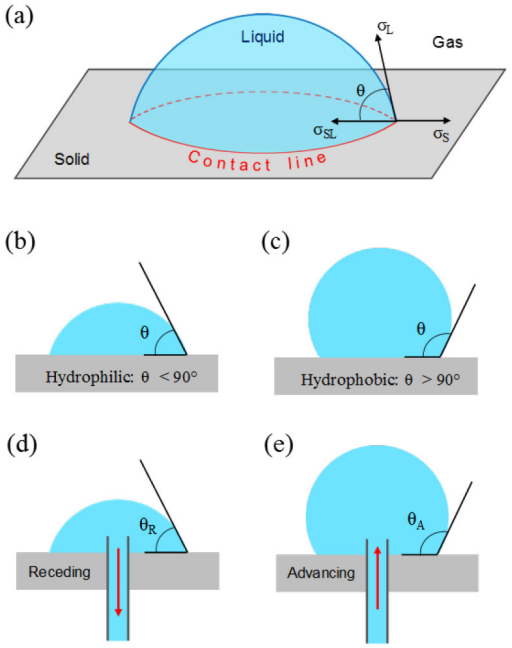

FIGURE 6. A three-phase system comprises a sessile droplet on a solid surface surrounded by a gas. The shape of the drop provides information about the wettability of the solid surface. (a) Equilibrium state caused by interfacial and surface tensions in a sessile droplet. The equilibrium contact angle θ is formed at the triple-phase contact line. (b) Wettable or hydrophilic surface, where the CA is between 0° and 90°. (c) Non-wettable or hydrophobic surface, where the CA is more than 90°. (d) Receding CA using the needle method. The droplet volume is gradually drawn using the tip of a needle. (e) Advancing CA using the needle method. The droplet volume is gradually increased through the use of the needle.

III. CAPILLARY BURST MICROVALVES THEORETICAL FRAMEWORK

The microfluidic reflectarray element design with capillary burst valve included segments of 700 µm in width and 1.5 mm in length, and interconnecting microchannels of 400 µm in width by 100 µm in length. The design was intended to demonstrate the control of the liquid metal within the microfluidic reflectarray element. The chips were fabricated using the lithographic technique described in section IV-B. The sudden expansion at the interconnecting microchannel ends as a capillary burst valve. The interconnections in the dipole act then as a series of capillary burst valves to control the advancement of the liquid metal as it flows within the microfluidic chip upon the application of external pressure. The basic operation of the microfluidic capillary burst valves is explained below. The flow rate inside the microchannels can be obtained using the Hagen-Poiseuille equation for laminar flow as follows:

$$Q = \left(\frac{\pi R^4}{8\nu}\right)\left(\frac{p_o - p_{int}}{l}\right) \tag{1}$$

where Q is the volumetric flow rate, R is the hydrodynamic radius of the microchannel, ν is the dynamic viscosity of the liquid, p_0 is the liquid pressure at the entrance of the microchannel, p_{int} is the liquid pressure at the interface (i.e., the meniscus), and l is the distance from the microchannel inlet to the air-liquid interface. Surface tension arising from the interaction between the liquid, gas, and solid phases is a key factor behind the microvalve principle of operation. Figure 6 illustrates a three-phase system sessile droplet forming a contact angle (CA) θ under equilibrium conditions. The surface energy of the solid σ_S acts along the solid surface, whereas the solid-liquid interfacial energy σ_{SL} acts in the opposite direction. The surface tension of the liquid σ_L acts tangential to the droplet's surface. For hydrophilic surfaces, the CA is less than 90° (Fig. 6b) and the meniscus at the air-liquid interface is driven by capillarity, whereas for hydrophobic surfaces, it is more than 90° (Fig. 6c) and the interface can only be advanced by an externally applied pressure. The advancing and receding contact angles were used to measure the dynamic CA of the three-phase system during motion. The advancing CA, illustrated in Fig. 6d, was measured during droplet expansion to provide information on the dry-wetting behavior of the solid-liquid interphase. A receding CA forms when the droplet volume decreases as the liquid is drawn, as illustrated in Fig. 6e. As detailed later, dynamic contact angles play an important role in stopping and enabling motion in a microfluidic burst valve.

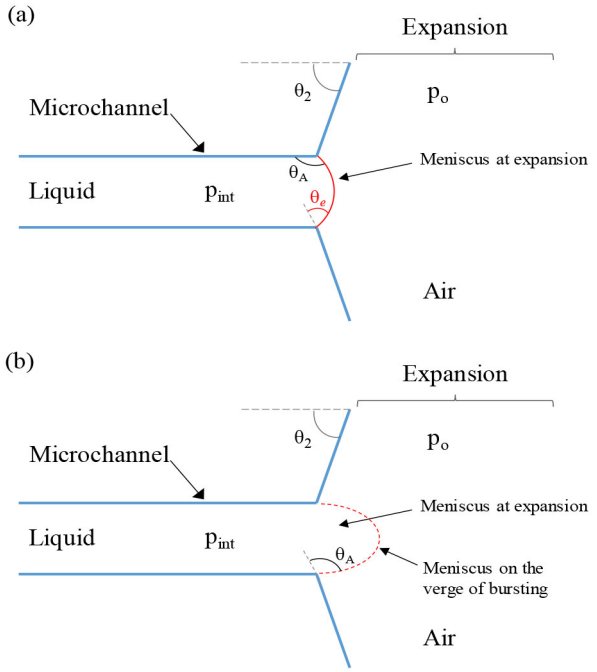

FIGURE 7. Schematic representation of a sudden microfluidic expansion. (a) Equilibrium meniscus state of the liquid at the sudden expansion, which causes a valving effect stopping the liquid. (b) Meniscus state at the verge of bursting due to an increase in the applied force (i.e., pressure difference). An infinitesimal increase in applied force results in the motion of the liquid into the expansion zone.

The Young-Laplace equation defines the capillary pressure in a three-phase system:

$$p_{atm} - p_{int} = \frac{2\sigma}{R} cos\theta \tag{2}$$

where p_{atm} is the atmospheric pressure or pressure outside the liquid, σ is the surface tension, and θ is the liquid-gas interface CA at the solid or static CA under equilibrium conditions. The pressure difference may result in the motion of a fluid within a microchannel, but the surface tension enables the fluid to stop at a sudden expansion on a non-wettable surface. To control the flow of liquid metal inside a microfluidic-based reconfigurable reflectarray, we propose the use of capillary burst microvalves that rely on sudden expansions to control the microflow of a liquid. Details of the physics behind the principle of operation of capillary burst microvalves have been presented in [23]. Fig. 7 shows a schematic of the microfluidic burst valves designed to control the flow of liquid metal in the reconfigurable reflectarrays. To stop the pressure-driven meniscus of the liquid metal, we propose using an abrupt expansion section (Fig. 7a). The pressure required to overcome the pinned liquid at the capillary burst microvalve is expressed by Eq. (2). It is convenient to introduce the critical advancing CA, θ_A, which is defined as the angle at which the triple line starts to move in the case of a sessile droplet on an inclined plane. The contact line cannot advance when the static or advancing contact angle is less than θ_A. When the liquid advances inside the microchannel, there is an apparent dynamic CA, θ_{aa}, which

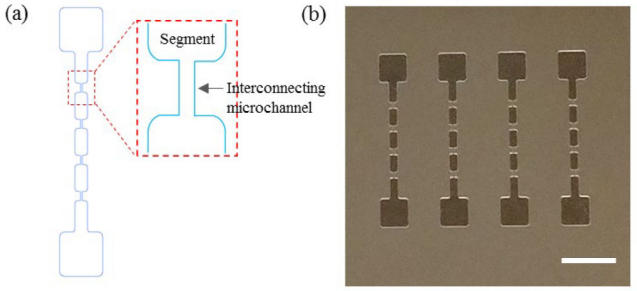

FIGURE 8. Microfluidic burst valve chip (a) CAD drawing used to produce the mask. (b) Fabricated master used to cast the PDMS chips. Scale bar represents 5 mm.

is a function of the meniscus velocity and θ_A and is inherently greater than θ. Under these conditions, θ_A and θ_{aa} are of the same order of magnitude, and the pressure difference required to advance the meniscus at the air-liquid interface can therefore be defined by Eq. (2), replacing θ by θ_A. When the meniscus encounters an abrupt geometric expansion, as illustrated in Fig. 7a, the CA is reduced to $\theta_e = \theta_A - \theta_2$, where θ_2 is the angle between the surface of the diverging expansion and the horizontal (Fig. 7b); therefore, $\theta_e = \theta_A - 90°$ for a sudden orthogonal expansion. The meniscus then stops when θ_A becomes greater than θ_e. This effect, which was first described for liquids encountering sharp solid edges [24], forms the basis of the capillary burst valve. For the meniscus to continue advancing, that is, for the valve to burst, the interface should bulge until θ_e reaches a value equal to θ_A. The new CA in the expansion relative to the microchannel wall increases from θ_A to $\theta_A + \theta_2$ [23]. However, 180° is the maximum CA that the meniscus can attain; therefore, if $\theta_A + \theta_2 > 180°$, the bursting conditions are reached when θ' equals 180°, and Eq. (2) becomes:

$$p_o - p_{int} = \Delta p_1 = \frac{2\sigma}{R} cos\theta' \tag{3}$$

where Δp_1 is lower than Δp_2, which prevents the advancement of the meniscus under these conditions unless the pressure difference increases sufficiently to burst the capillary effect. The meniscus moved within the expansion section once the pressure difference exceeded and the capillary valve burst. As the CA of the meniscus advances, the pressure across the air-liquid interface in the expansion section is defined by the new CA with respect to the expansion wall. These principles and considerations were used to design the microfluidic chip shown in Fig. 8a. They were used as a proof-of-concept for the control of Galinstan within the different sections of the microchannels via capillary burst microvalves.

For a liquid interface inside a rectangular channel, considering the advancing CA at the side walls and at the upper and bottom walls θ_{a1} and θ_{a2}, respectively, the Young-Laplace equation yields [15]

$$p_o - p_{int} = \Delta p_2 = 2\sigma \left(\frac{cos\theta_{a1}}{w} + \frac{cos\theta_{a2}}{h} \right) \tag{4}$$

where w and h are the width and height of the microchannels, respectively. In this case, the conditions for the meniscus to advance are similar, where both θ_{a1} and θ_{a2} must be greater than θ_A, and the pressure difference at the bulging interface based on the Young-Laplace equation becomes

$$p_o - p_{int} = \Delta p_2 = 2\sigma\left(\frac{cos\theta}{w} + \frac{cos\theta_A}{h}\right) \tag{5}$$

And the interfacial pressure on the verge of capillary bursting is then:

$$p_o - p_{int} = \Delta p_2 = 2\sigma\left(\frac{cos\theta'_{new}}{w'} + \frac{cos\theta_A}{h}\right) \tag{6}$$

where w' denotes the width of the expansion section. In the next section, we present the design and fabrication of a simplified version of the microfluidic reconfigurable reflectarray, including capillary-burst microvalves.

IV. CAPILLARY BURST VALVES AND RF PROOFS-OF-CONCEPT TOWARDS MICROFLUIDIC RECONFIGURABLE REFLECTARRAY ANTENNAS

To demonstrate the potential of the proposed technology, two proofs of concept were independently implemented and successfully tested in the laboratory.

A. CAPILLARITY BURST VALVES PROOF-OF-CONCEPT

The design of the mechanical proof-of-concept for controlling the flow of liquid metal within the microchannels of a reflectarray element is illustrated in Fig. 8a. The fabrication of the masters (i.e., molds) with microfluidic-based elements and discrete structures was achieved using a lithographic technique at the Nanofabrication Kingston facility (NFK, Innovation Park, Kingston, Ontario). This technique is widely used in microfluidic applications and enables the creation of microfluidic chips by replica molding. The general steps of the fabrication procedure are described below.

A computer-aided design (CAD) mask model with the microfluidic pattern was generated using the SolidWorks software (SolidWorks Corp., Dassault Systèmes, USA). The layer thickness for all internal microfluidic components was 30 μm. A master was fabricated by spin-coating an SU-8 50 photoresist (MicroChem Corp., Newton, MA, USA) onto a clean 4-inch single-side-polished silicon wafer. The coated wafer was then pre-baked at 65 °C and 95 °C for 2 and 8 min, respectively. The mask with a microfluidic design was then placed over the coated wafer and exposed to UV light for 90 s. Next, the exposed wafer was hard-baked at 65 °C for 1 min and 95 °C for 10 min. The master was subsequently developed using SU-8 developer (MicroChem Corp., Newton, MA, USA). The resulting master of the microfluidic design with capillary burst microvalves is shown in Fig. 8b.

A 13:1 mixture of Sylgard 184 elastomer and curing agent (Dow Corning, Midland, MI) was mixed, degassed in vacuum, and poured onto the master. After baking at 85 °C for 20 min, the replica peeled off from the mold. Although the lithographic method used here is reliable and well established, 3D printing technologies could be an alternative to fabricate molds for microfluidic chips.

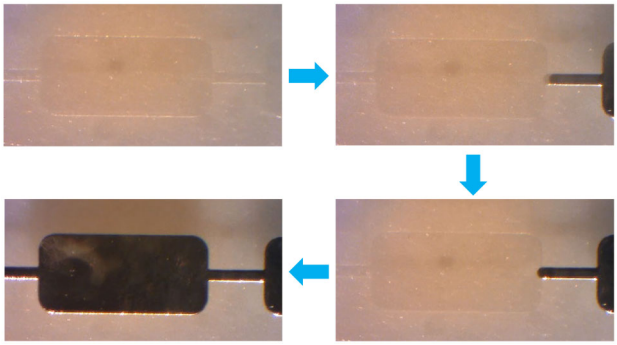

FIGURE 9. Testing of the capillary burst microvalves. The image sequence shows the chip before being filled with Galinstan (upper left); the subsequent filling of the segment and microchannel (upper right) upon the application of an external pressure; the pinning of the liquid-metal meniscus at the abrupt expansion (bottom right); and the filling of the entire dipole by increasing the applied pressure.

The microfluidic burst valve chip was tested by introducing Galinstan into the chip by punching two holes through PDMS, acting as the inlet and outlet, and connecting the inlet to a syringe using PEEK tubing of 1/32" ID. The chip was flushed with 0.3mol/L sodium hydroxide (NaOH) solution, and Galinstan was then introduced into the microstructure with the aid of a syringe. Fig. 9 shows the image sequence of the introduction and advancement of liquid metal. Upon applying of external pressure, it fills the first segment of the chip and then flows into the interconnecting microchannel. The meniscus stopped and was pinned at an abrupt expansion (bottom right). The applied pressure was increased to produce a bulging of the interface, and the capillary valve finally burst, filling the entire dipole at ∼130 ms (1 frame at 7.5 fps). This proof-of-concept proves that the proposed microfluidic reflectarray element incorporating capillary burst valves effectively control the liquid metal advancement.

B. RADIOFREQUENCY PROOF-OF-CONCEPT

Additional microfluidic designs of discrete elements that correspond, in length and volume, to different numbers of segments filled with Galinstan were also fabricated for use as a radiofrequency proof-of-concept and to verify the feasibility of the proposed technology as a reflectarray element. Fig. 10(a) and (b) show the microfluidic chips before and after filling with Galinstan, respectively. The samples were fabricated using dipoles of different lengths: 3.61 mm, 4.50 mm, 5.20 mm. mm, respectively, and their widths and thickness are 0.68 mm and 0.10 mm, respectively. The PDMS bottom layer thickness, in which the Galinstan cavity was embedded, was 1.8 mm, while the top layer thickness was 0.3 mm. The capilars used to fill the metal liquid have a diameter of 0.68 mm and remain also filed. These capilars are responsible for phase inversion in the response, and the quantity of Galinstan inside also impacts on the phase value.

The well-known waveguide simulator technique [25], in which a discrete number of elements (in this case, two

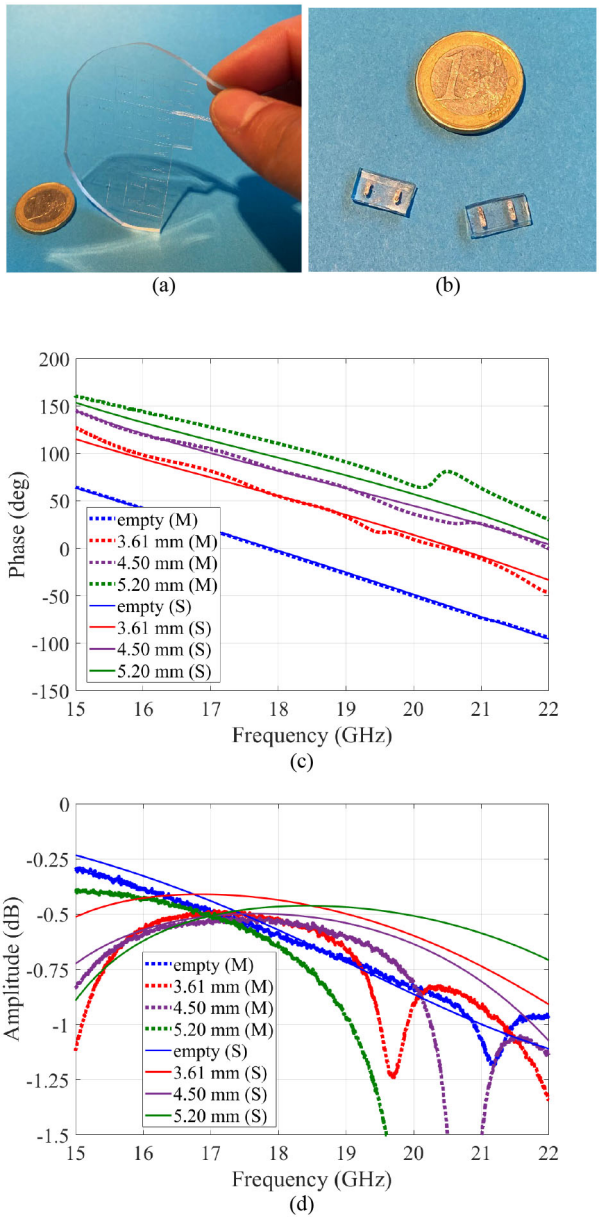

FIGURE 10. Discrete microfluidic dipole elements used to obtain the reflected wave as a function of the dipole length. (a) fabricated microfluidic before cutting and filling. (b) discrete elements with Galinstan. (f) Measured (M) and simulated (S) phase of the reflection coefficient using a WR51 waveguide for empty cell and different lengths of dipole: 3.61 mm, 4.50 mm and 5.20 mm (d) Measured (M) and simulated (S) amplitude for the reflection coefficient for the same samples.

identical dipoles) are introduced in a short-circuited waveguide, which is connected to one port of the VNA, to measure the reflection coefficient. This experimental validation was performed using the WR51 waveguide (15 – 22 GHz), whose dimensions allow simple handling of the samples in the waveguide. However, the proposed technology can be used at higher frequencies as long as the fabrication tools are available. Fig. 10(c) shows the measured (M) and simulated (S) phases for the reflected wave as a function of the frequency for different dipole lengths, demonstrating the feasibility of using the proposed technology in future reconfigurable reflectarray antennas. The experimental data for the phase were in good agreement with the simulations, except for the larger dipole, where an almost constant difference was observed. This difference can be attributed to the quantity of Galinstan inside the capilars, which seems to have less fluid than in the other samples. Both the measured and simulated average losses are in an average range of 0.5 dB, from 15 GHz to 19 GHz, with a maximum of 1 dB, as can be seen in Fig. 10(d). The largest discrepancy can again be observed for the 5.20 mm sample. These losses are incremented at higher frequencies because of unexpected resonance in the waveguide, which can be explained by an air gap between the back PDMS and the ground plane. As expected, the phase response shows linear behavior, which is a desirable feature in this type of element, and it was observed that the empty elements have similar responses between them independent of the length of the air groove.

V. CONCLUSION

Microfluidics-based technology is an interesting alternative for implementing multi-reconfiguration in electromagnetic systems. This paper proposes an optimized design of a new microfluidic-based chip, along with the use of a non-toxic liquid metal alloy, as an efficient mechanism for dynamically controlling the frequency or phase of reflectarray elements. Two potential elements were proposed. The aperture coupled element allows for an efficient reconfiguration of the operation frequency, whereas the dipole-based element allows reconfiguration of the phase of the reflected wave. Both elements can be further optimized to implement multi-reconfiguration, which means dynamically changing at the same, at least two of the main features of the element: frequency, polarization, and phase. The capillary action of an abrupt microfluidic expansion is used as a capillary burst valve to control the flow of the liquid metal in the microfluidic chip. A proof-of-concept of the required microfluidic technology has been introduced from both mechanical and radiofrequency points of view, demonstrating promising results. Improving the accuracy of the cavity thickness and width, which directly impacts on the phase range or the actuation method in a full antenna, is an open subject for further research. The proposed method opens a new avenue for reconfigurable reflectarray elements that can be further reduced in scale, customized, and parallelized to satisfy the requirements of fast-evolving applied electromagnetics, particularly antennas and sensors.

REFERENCES

[1] J. Huang and J. A. Encinar, *Reflectarray Antennas*. Hoboken, NJ, USA: Wiley, 2007.

[2] S. V. Hum and J. Perruisseau-Carrier, "Reconfigurable reflectarrays and array lenses for dynamic antenna beam control: A review," *IEEE Trans. Antennas Propag.*, vol. 62, no. 1, pp. 183–198, Jan. 2014, doi: 10.1109/TAP.2013.2287296.

[3] J. Perruisseau-Carrier, "Dual-polarized and polarization-flexible reflective cells with dynamic phase control," *IEEE Trans. Antennas Propag.*, vol. 58, no. 5, pp. 1494–1502, May 2010, doi: 10.1109/TAP.2010.2044333.

[4] D. Rodrigo, L. Jofre, and J. Perruisseau-Carrier, "Unit cell for frequency-tunable beamscanning reflectarrays," *IEEE Trans. Antennas Propag.*, vol. 61, no. 12, pp. 5992–5999, Dec. 2013, doi: 10.1109/TAP.2013.2281375.
[5] C. Escobedo, "On-chip nanohole array based sensing: A review," *Lab. Chip*, vol. 13, pp. 2445–2463, Mar. 2013, doi: 10.1039/C3LC50107H.
[6] G. M. Whitesides, "The origins and the future of microfluidics," *Nature*, vol. 442, pp. 368–373, Jul. 2006, doi: 10.1038/nature05058.
[7] N. A. Polson and M. A. Hayes, "Microfluidics: Controlling fluids in small places," *Anal. Chem.*, vol. 73, pp. 312–319, Jun. 2001, doi: 10.1021/ac0124585.
[8] A. Arbelaez, I. Goode, J. Gomez-Cruz, C. Escobedo, and C. E. Saavedra, "Liquid metal reconfigurable patch antenna for linear, RH, and LH circular polarization with frequency tuning," *Can. J. Elect. Comput. Eng.*, vol. 43, no. 4, pp. 218–223, 2020, doi: 10.1109/CJECE.2019.2904898.
[9] M. Borhani, P. Rezaei, and A. Valizade, "Design of a reconfigurable miniaturized microstrip antenna for switchable multiband systems," *IEEE Antennas Wireless Propag. Lett.*, vol. 15, pp. 822–825, 2016, doi: 10.1109/LAWP.2015.2476363.
[10] S.-J. Wu and T.-G. Ma, "A wideband slotted bow-tie antenna with reconfigurable CPW-to-slotline transition for pattern diversity," *IEEE Trans. Antennas Propag.*, vol. 56, no. 2, pp. 327–334, Feb. 2008, doi: 10.1109/TAP.2007.915454.
[11] S. A. Long and G. H. Huff, "A fluidic loading mechanism for phase reconfigurable reflectarray element," *IEEE Antennas Wireless Propag. Lett.*, vol. 10, pp. 876–879, 2011, doi: 10.1109/LAWP.2011.2165930.
[12] K. Khoshmanesh *et al.*, "Liquid metal enabled microfluidics," *Lab Chip*, vol. 17, pp. 974–993, Feb. 2017, doi: doi.org/10.1039/C7LC00046D.
[13] D. L. Diedhiou, D. Iero, O. de Sagazan, R. Sauleau, and A. V. Boriskin, "Inset-Fed liquid metal patch antenna," in *Proc. 8th Eur. Conf. Antennas Propag. (EuCAP)*, The Hague, The Netherlands, Apr. 2014, p. 1720, doi: 10.1109/EuCAP.2014.6902128.
[14] N. S. Jeong and A. Koh, "Liquid metal broadband monopole for stretchable electronics," in *Proc. IEEE Int. Symp. Antennas Propag. USNC-URSI Radio Sci. Meeting*, 2019, pp. 763–764, doi: 10.1109/APUSNCURSINRSM.2019.8888557.
[15] Z. Chen, H. Wong, J. Xiang, and J. Kelly, "Polarization reconfigurable antenna with liquid," in *Proc. IEEE Int. Conf. Comput. Electromagn. (ICCEM)*, 2018, pp. 1–3, doi: 10.1109/COMPEM.2018.8496613.
[16] G. Zhang, R. C. Gough, M. R. Moorefield, and K. Cho, "A liquid-metal polarization-pattern-reconfigurable dipole antenna," *IEEE Antennas Wireless Propag. Lett.*, vol. 17, no. 1, pp. 50–53, Jan. 2018, doi: 10.1109/LAWP.2017.2773076.
[17] M. Riel and J.-J. Laurin, "Design of an electronically beam scanning reflectarray using aperture-coupled elements," *IEEE Trans. Antennas Propag.*, vol. 55, no. 5, pp. 1260–1266, May 2007, doi: 10.1109/TAP.2007.895586.
[18] E. Carrasco, M. Barba, and J. A. Encinar, "X-band reflectarray antenna with switching-beam using in diodes and gathered elements," *IEEE Trans. Antennas Propag.*, vol. 60, no. 12, pp. 5700–5708, Dec. 2012, doi: 10.1109/TAP.2012.2208612.
[19] O. Bayraktar, O. A. Civi, and T. Akin, "Beam switching reflectarray monolithically integrated with RF MEMS switches," *IEEE Trans. Antennas Propag.*, vol. 60, no. 2, pp. 854–862, Feb. 2012, doi: 10.1109/TAP.2011.2173099.
[20] J. Zang, E. Carrasco, X. Wang, A. Alvarez-Melcon, and J. S. Gomez-Diaz, "Analysis and design of reflectarray antennas based on delay lines: A filter perspective," *IEEE Access*, vol. 8, pp. 44947–44956, 2020, doi: 10.1109/ACCESS.2020.2976643.
[21] E. Carrasco, M. Barba, J. A. Encinar, M. Arrebola, F. Rossi, and A. Freni, "Design, manufacture and test of a low-cost shaped-beam reflectarray using a single layer of varying-sized printed dipoles," *IEEE Trans. Antennas Propag.*, vol. 61, no. 6, pp. 3077–3085, Jun. 2013, doi: 10.1109/TAP.2013.2254431.
[22] G. Perez-Palomino *et al.*, "Design and demonstration of an electronically scanned reflectarray antenna at 100 Ghz using multiresonant cells based on liquid crystals," *IEEE Trans. Antennas Propag.*, vol. 63, no. 8, pp. 3722–3727, Aug. 2015, doi: 10.1109/TAP.2015.2434421.
[23] H. Cho, H.-Y. Kim, J. Y. Kang, and T. S. Kim, "How the capillary burst microvalve works," *J. Colloid Interface Sci.*, vol. 306, no. 2, pp. 379–385, Feb. 2007, doi: 10.1016/j.jcis.2006.10.077.
[24] J. W. Gibbs, *The Scientific Papers*. New York, NY, USA: Dover, 1961.
[25] P. W. Hannan and M. A. Balfour, "Simulation of a phased-array antenna in waveguide," *IEEE Trans. Antennas Propag.*, vol. AP-13, no. 3, pp. 342–353, May 1965, doi: 10.1109/TAP.1965.1138428.

EDUARDO CARRASCO (Senior Member, IEEE) received the bachelor's degree in telecommunication engineering from the National Autonomous University of Mexico, Mexico City, in 2000, and the Ph.D. degree in telecommunication engineering from the Technical University of Madrid (UPM), Spain, in 2008. From January to April 2008, he visited the Microwave Engineering Laboratory with the University of Perugia, Italy. From June 2009 to June 2012, he was employed with the Electromagnetism and Circuits Theory Department, UPM, Spain, as a Postdoctoral Researcher, where he participated in various projects supported by the Spanish Government, the Mexican Council of Science and Technology (CONACYT), the European Union's Sixth and Seventh Framework (FP6 and FP7) Programs, and the European Space Agency. From 2012 to 2014, he was with the Swiss Federal Institute of Technology, Lausanne, Switzerland, as a Marie-Curie Fellow. He was with the Foundation for Research on Information Technologies in Society (IT'IS Foundation), Zurich, Switzerland, from January 2015 to September 2017, as a Electromagnetic, Dosimetry, and Antenna Engineer. Since October 2017, he has been with Information Processing and Telecommunications Center, UPM, Madrid, Spain, where he is currently an Associate Professor. His main research interests include the design of reconfigurable antenna arrays, including reflect- and transmit-arrays, from microwave to terahertz frequencies, as well as EMF exposure, hyperthermia treatment planning and other bioelectromagnetics topics.

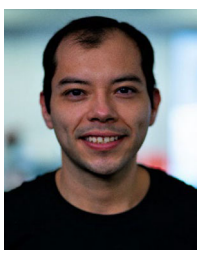

JUAN GOMEZ-CRUZ (Member, IEEE) received the B.Sc. degree in communications and electronics engineering from Instituto Politécnico Nacional, Mexico, the M.Sc. degree in electrical engineering from Universidad Nacional Autónoma de México, Mexico (UNAM), and the Ph.D. degree in electrical engineering and chemical engineering from UNAM and Queen's University, Canada, respectively. He is currently a Mitacs Industrial Postdoctoral Fellow with Queen's University and Spectra Plasmonics Inc. During his Ph.D. degree, he worked on the development of biosensors based on plasmonic effects in nanostructured metallic films. His research focuses on the theoretical and experimental design and construction of highly sensitive, handheld sensing platforms based on surface plasmon resonance for point-of-care diagnostics.

MARIO SERRANO-BERRUECO received the master's degree in telecommunication engineering from Universidad Politécnica de Madrid in 2020. He is currently with the private industry.

CARLOS E. SAAVEDRA received the Ph.D. degree in electrical engineering from Cornell University, Ithaca, New York. He is currently a Full Professor and Head of the Department of Electrical and Computer Engineering with Queen's University, Kingston, ON, Canada. He has served as the Co-Chair of the Natural Sciences and Engineering Research Council of Canada Discovery Grant Evaluation Group for Electrical and Computer Engineering and has also served grant review panels at the National Science Foundation (USA). He is a Former Associate Editor of the IEEE TRANSACTIONS ON MICROWAVE THEORY AND TECHNIQUES and the Guest Editor of the IEEE OPEN JOURNAL OF ANTENNAS AND PROPAGATION and the *IEEE Microwave Magazine*.

CARLOS ESCOBEDO (Member, IEEE) received the B.Sc. degree from the National University of Mexico, the M.A.Sc. degree from the University of Toronto, and the Ph.D. degree from the University of Victoria. He is an Associate Professor with the Department of Chemical Engineering, with Cross-Appointment to the Department of Chemistry, Queen's University, and the Department of Physics and Space Science, Royal Military College of Canada. His research focuses on the development of nanostructured (bio)sensors and microfluidic platforms for analytical applications in biomedicine, chemistry and telecommunications. He was a NSERC Postdoctoral Fellow with Bioengineering Laboratory, ETH Zürich, Switzerland, from 2011 to 2013, and has four years of experience in the medical R&D industry, working for Innovamedica as Head of Mechanical Engineering. He joined Queen's University in May 2013; and served for four years as Chair of Nanotechnology and Microfluidics in the Canadian Society for Mechanical Engineering. He is the recipient of an Ontario Early Researcher Award, a Queen's Excellence in Research Award and was honored with the TD Bank's 10 Most Influential Hispanic Canadians Award, which recognizes 10 outstanding Hispanic-Canadians from across Canada.